Synthesis and characterization of a nano-scaled barium cerate perovskite powder using starch as polymerization agent

Roberto Köferstein, Dietrich Hesse, Stefan G Ebbinghaus

Solid State Ionics 203 (2011) 52–56

(doi:10.1016/j.ssi.2011.09.010)

http://dx.doi.org/10.1016/j.ssi.2011.09.010

Synthesis and characterization of a nano-scaled barium cerate perovskite powder using starch as polymerization agent

Roberto Köferstein[a,*], Dietrich Hesse[b], Stefan G. Ebbinghaus[c]

[a]*Department of Environmental Engineering, Helmholtz Centre for Environmental Research – UFZ, Permoserstr. 15, 04318 Leipzig, Germany.*

[b]*Max Planck Institute of Microstructure Physics, Weinberg 2, 06120 Halle, Germany.*

[c]*Institute of Chemistry, Inorganic Chemistry, Martin-Luther-University Halle-Wittenberg, Kurt-Mothes-Strasse 2, 06120 Halle, Germany.*

* Corresponding author. Tel.: +49-341-2351698; Fax: +49-341-2351471.
E-mail address: roberto_koeferstein@web.de

Abstract. The preparation of nano-sized $BaCeO_3$ powder using starch as a polymerization agent is described herein. Phase evolution during the decomposition process of a (BaCe)-gel was monitored by XRD. A phase-pure nano-sized $BaCeO_3$ powder was obtained after calcining of the (BaCe)-gel at 920 °C. The resulting powder has a specific surface area of 15.4 m^2/g. TEM investigations reveal particles mainly in the size range of 30 to 65 nm. The shrinkage and sintering behaviour of resulting powder compacts were studied in comparison to a coarse-grained mixed-oxide $BaCeO_3$ powder (S_{BET} = 2.1 m^2/g). Dilatometric measurements show that the beginning of shrinkage of compacts from the nano-sized powder

is downshifted by 300 °C compared to mixed-oxide powder. Compacts from the nano-sized powder reach a relative density of 91 % after sintering at 1450 °C for 10 h.

Keywords: *barium cerate; starch; perovskite; ceramic; sintering; soft-chemistry synthesis*

1. Introduction

Perovskite materials based on $BaCeO_3$ possess high proton conductivity in humid atmospheres between 600 and 800 °C. Therefore, $BaCeO_3$ based compounds have potential for energy-related applications and they are candidates as electrolyte materials for solid oxide fuel cells (SOFCs) [1,2,3,4,5,6,7]. $BaCeO_3$ based materials are unstable in CO_2 and H_2O containing atmospheres [8,9], which limits the applications for SOFCs. However, *Katahira* et al. [4] improved the chemical stability in a CO_2 environment using Zr^{4+} as dopant. An enhanced chemical stability against CO_2 and water was found both in the systems $BaCe_{0.7}Nb_{0.1}Sm_{0.2}O_{3-\delta}$ [10] and $BaIn_{0.1}Y_{0.2}Ce_{0.7}O_{3-\delta}$ [11].

Furthermore, barium cerate can be also applied as a functional material for semiconductor gas sensors [12] and solid solutions of the type $BaTi_{1-x}Ce_xO_3$ can be used for capacitor applications [13,14,15,16,17].

Catalytic activity of $BaCeO_3$ on the oxidation of methane was investigated by *Benlhachemi* et al. [18] and *Popescu* et al. [19]. A $BaCeO_3$ supported ruthenium catalyst shows excellent activity for ammonia synthesis as reported by *Yang* et al. [20]. Additionally, soot oxidation activity and an improved tolerance to SO_2 poisoning were found on an $Ag/BaCeO_3$ catalyst [21]. *Yuan* et al. [22] examined the photocatalytic water splitting properties of $BaCeO_3$.

$BaCeO_3$ crystallizes in the perovskite structure and exhibits three phase transitions up to 1000 °C as reported by *Knight* [23] and *Genet* et al. [24]. A first transition at 290 °C leads from a

primitive orthorhombic perovskite structure (space group: Pmcn) to the body-centred one (Incn), a second at 400 °C to a rhombohedrally distorted one ($R\bar{3}c$) and the last transition at 900 °C to the cubic perovskite structure ($Pm\bar{3}m$).

Compacts on the basis of $BaCeO_3$ generally reveal only a moderate densification behaviour [4,25]. For application such as capacitors or in SOFCs the density of the ceramics must be high [26,27,28,29,30,31]. On the other hand, sintering temperatures above 1500 °C should be avoided because $BaCeO_3$ melts incongruently at 1480 °C ± 5 °C with the formation of CeO_2 and a liquid containing BaO [5,32].

In general, powders with high specific surface areas can improve the catalytic activity, the densification behaviour of compacts, and lead to ceramic bodies with a fine-grained microstructure [33,34,35]. *Kim* et al. [36] reported on the effect of fine- and coarse-grained $BaCeO_3$ on the microstructure and the critical current density of a melt-textured $YBa_2Cu_3O_{7-y}$. Since the mixed-oxide method mostly results in coarse-grained powders some wet chemical syntheses have been developed to obtain fine-grained or nano-scaled $BaCeO_3$ powders such as various precursor complex methods, solvothermal- and sol-gel syntheses [29,37,38,39,40,41,42]. Nano-sized powders via Pechini based routes are reported by *Lee* at al. [43], *Osman* et al. [44] and *Su* et al. [45]. A hydrothermal process using urotropine [46], a sol-gel combustion [47] and an acrylate hydrogelation method [48] lead also to nano-$BaCeO_3$ powders. Almost all of those preparation methods use Ce^{3+}-compounds as starting materials to obtain $BaCeO_3$. On the other hand, it seem to be advantageous to use Ce^{4+}-based starting materials to synthesize $BaTi_{1-x}Ce_xO_3$ solid solutions by wet chemical methods [49].

The aim of this paper is to describe a simple and cheap one-pot synthetic route starting from a Ce^{4+}-compound and using starch as a polymerization agent to obtain nano-sized $BaCeO_3$. We use starch because of its eco friendly character and is a cheap abundant biopolymer. We have examined the phase evolution during the decomposition process. The shrinkage behaviour of resulting $BaCeO_3$ compacts has also been determined.

2. Experimental

2.1. Material preparation

$Ba(CH_3COO)_2$ (0.01 mol, *Merck*) and $(NH_4)_2Ce(NO_3)_6$ (0.01 mol, *Alfa Aesar*) were separately dissolved in 20 ml water. 6 g soluble starch (M = 324.30 g/mol, *Sigma-Aldrich*) were suspended under stirring in 20 ml water on a heating plate at 100 °C. After 5 min the barium acetate solution was added together with further 3 g starch. The mixture was stirred and after 5−10 min the temperature of the heating plate was raised to 120 °C. Under stirring the $(NH_4)_2Ce(NO_3)_6$ solution was slowly added. The resulting mixture was stirred and heated until it became a high viscous orange gel. The gel turned to a light yellow after about 15 min.

The obtained (BaCe)-gel was calcined in static air at 920 °C for 2 h by a heating rate controlled thermal treatment to yield a nano-sized $BaCeO_3$ powder (**1**), as described below. Powder **1** was mixed with 5 mass% of a saturated aqueous solution of polyvinyl alcohol (PVA) as a pressing aid, then the powder was pressed into pellets to a green density of about 2.6 g/cm^3.

For comparative purposes, a coarse-grained $BaCeO_3$ powder (**2**) was prepared via a conventional mixed-oxide method and the resulting compacts had a green density of about 3.5 g/cm^3 as described and investigated elsewhere [25].

2.2. Characterization

X-ray powder diffraction (XRD) patterns were recorded on a *STOE* STADI MP diffractometer at room temperature using Co−$K\alpha_1$ radiation. Powder patterns were refined with the profile fitting software PowderCell [50]. Crystallite sizes were determined by XRD line broadening using the Scherrer equation [51] and the integral peak breadth (software suite WinXPOW [52]). The Wilson-equation was used to determine the strain parameter [52,53]. Dilatometric investigations (shrinkage) were performed in a flowing synthetic air atmosphere

(50 ml/min) in a *Setaram* TMA 92-16.18 dilatometer. Simultaneous thermogravimetric (TG) and differential thermoanalytic (DTA) measurements were achieved in flowing air (30 ml/min) with heating rates of 10 and 1 K/min up to 1200°C using a *Netzsch* STA 449 System. The TG/DTA measurements of the decomposition of the (BaCe)-gel was carried out on a sample preheated at 250 °C for 0.5 h. The specific surface area was determined using nitrogen three-point BET (Nova 1000, *Quantachrome Corporation*). The equivalent BET particle diameter was calculated assuming the powder particles were spherical or cubic in shape [54]. Transmission electron microscopy (TEM) samples were prepared by dispersing the powder in alcohol under ultrasonic agitation, and collecting it onto a copper TEM grid covered with a carbon membrane. TEM images were recorded with a *Philips* CM20Twin at an electron energy of 200 keV.

3. Results and discussion

3.1. Powder characterization

Simultaneous TG and DTA investigations were carried out on a (BaCe)-gel preheated at 250 °C for 0.5 h to obtain a slightly hygroscopic black powder. At a fast heating rate of 10 K/min (Fig. 1a) we observed a slight weight loss of 4.6 % up to 246 °C accompanied by a weak endothermic signal. This weight loss is caused by adsorbed water due to the storage of the preheated sample in ambient atmosphere. At higher temperatures a three-step decomposition process until 381 °C led a weight loss of 68.1 %, resulting in the formation of orthorhombic $BaCO_3$ and cubic CeO_2 as main products [55] (see also Fig. 2). These processes are accompanied by a weak exothermic DTA signal at 253 °C (onset) and two intense and sharp DTA peaks with onset temperatures of about 317 and 341 °C (Fig. 1b). The exothermic peaks at 317 and 341 °C suggest a self-combustion-like process in which the nitrate ions act as an oxidizing agent, the starch and the acetate ions as fuels. Between 741 and about 995 °C there is a last weight loss step caused by the reaction of $BaCO_3$ and CeO_2 to $BaCeO_3$. The total

weight loss is 76.1 %. TG/DTA investigations with a slow heating rate of 1 K/min show that the beginning of the several decomposition steps is shifted to lower temperatures. The beginning of the self-combustion reaction is characterized by a very sharp exothermic signal with an onset temperature of about 282 °C and a shoulder at 299 °C. The last decomposition step starts at 665 °C and is finished at 880 °C. The total weight loss of 77.8 % is slightly higher than for the measurement with 10 K/min. The difference in the total weight losses between both measurements is caused by the slightly hydroscopic nature of the black preheated sample. In both cases the white TG/DTA residues were identified as orthorhombic $BaCeO_3$.

Fig. 2 shows the phase evolution during the thermal decomposition of the yellow amorphous (BaCe)-gel (Fig. 2a). For these XRD investigations the samples of the (BaCe)-gel were heated in a muffle furnace in static air at various temperatures for 1 h (heating rate 10 K/min) resulting in fluffy powders. Calcination at 300 °C, i.e. below the ignition temperature of the self-combustion process, yielded a black powder showing only reflections of cubic $Ba(NO_3)_2$ [55] (Fig. 2b). The reflections of $Ba(NO_3)_2$ disappear at 400 °C and the resulting yellow powder reveals the diffraction patterns of orthorhombic $BaCO_3$ and cubic CeO_2 [55] (Fig. 2c). With increasing calcination temperature the resulting powders gradually turn into a white colour. Since the strongest reflection (111) at about $2\theta = 33.2°$ of cubic CeO_2 overlaps with the strongest reflections of orthorhombic $BaCeO_3$ (020/211) it is difficult to determine the beginning of the formation of $BaCeO_3$. A heat treatment at 900 °C shows the evolution of reflections at $2\theta = 47.9°$ and 59.6° which do not belong to CeO_2 indicating definitely the formation of $BaCeO_3$ [55] (Fig. 2f). Decomposition at 1000 °C for 1 h leads to a powder revealing only reflections of orthorhombic $BaCeO_3$ (Fig. 2g).

According to the TG/DTA investigations the temperature for the formation of $BaCeO_3$ depends on the heating rate and soaking time. To obtain a phase pure nano-sized $BaCeO_3$ powder (see Fig. 2h) we calcined the (BaCe)-gel by the following optimised thermal

treatment in static air: heating to 500 °C with a heating rate of 10 K/min, slow heating with 1 K/min to 920 °C, holding at this temperature for 2 h and cooling with 3 K/min to room temperature. The white fluffy powder (**1**) obtained by this procedure has a specific surface area of S_{BET} = 15.4 m^2/g corresponding to an equivalent particle size of 61 nm, which can be considered the average size of the primary particles [56]. We calculated the crystallite size of powder **1** as 41 nm using the Scherrer equation, representing a volume-weighted average crystallite size [51]. According to the Wilson-equation [53] the root-mean-square-strain was found to be 0.002. The calculated crystallite size is slightly smaller than the size of the primary particles obtained from the BET data, because the calcination procedure of the (BaCe)-gel leads to closely joined crystallites and surface areas unavailable for nitrogen adsorption, as described elsewhere [57,58]. TEM investigations (Fig. 3) of powder **1** mainly show particles in the range of 30 to 65 nm, which are generally agglomerated. Isolated particles up to about 85 nm are also observed. Recently, *Bhowmick* et al. [46] synthesized nano-$BaCeO_3$ by a wet chemical method using urotropine. After heating at 800 °C for 10 h they obtained $BaCeO_3$ with an average crystallite size of 75 nm. A combination of both solvothermal and annealing processes at 900 °C was reported by *Chao* et al. [39], which resulted in a $BaCeO_3$ powder with particles of about 80 nm.

The XRD pattern of the nano-scaled $BaCeO_3$ powder **1** (corrected by an internal standard) was refined on the basis of a primitive orthorhombic unit cell (Pmcn) according to *Knight* et al. [59,23]. We calculated the unit cell parameters as a= 877.19 pm, b= 624.22 pm, c= 620.78 pm, V= $339.91 \cdot 10^6$ pm^3. These lattice constants correspond well to previously reported data for pure $BaCeO_3$ [59,23].

For comparison purposes we also investigated a coarse-grained $BaCeO_3$ powder (**2**) as described elsewhere [25]. That powder results from a conventional mixed-oxide process at 1150 °C for 4 h and has a specific surface area of 2.1 m^2/g and thus an equivalent particle size of 449 nm.

3.2. Sintering behaviour and phase transition

Fig. 4 shows the non-isothermal dilatometric investigations up to 1500 °C. Since the green compacts **1** (2.6 g/cm^3) and **2** (3.5 g/cm^3) differ in their densities the values of the relative shrinkage are not directly comparable. Therefore, from the relative shrinkages the evolution of the relative densities depending on temperature was calculated assuming an isotropic shrinkage of the compacts.

Sample **1** begins to shrink at about 920–940 °C and shows a broad peak in the shrinkage rate curve (inset in Fig. 4) with a maximum at 1290 °C (rate: -1.0 %/min). The calculated densification increases up to a relative density of 85 % at 1500 °C. The shrinkage of the coarse-grained compact **2** starts at about 1230 °C and shows two maxima of the shrinkage rate at 1383 °C and at 1456 °C with lower rates of -0.22 %/min and -0.33 %/min, respectively [25]. The densification reaches a value of only 61 % of the relative density up to 1500 °C. The shrinkage rates of sample **1** and **2** indicate that the densification is dominated by sliding processes, because diffusion processes would have only effected the shrinkage rate by less than 0.1 %/min [60,61,62].

The development of the final bulk densities of ceramic bodies of **1** and **2** after isothermal sintering at various temperatures with a soaking time of 10 h is represented in Fig. 5. The bulk densities of the sintered bodies were calculated from their weight and geometric dimensions. The relative bulk densities of the ceramic bodies refer to the single crystal density of 6.36 g/cm^3 [59]. Coarse-grained powder compacts of **2** show an insufficient sintering behaviour. Even after sintering at 1500 °C for 10 h we do not obtain any dense ceramic bodies but the relative densities remained below 77 % [25]. In contrast, compacts made from the nano-sized powder **1** exhibit an improved sintering behaviour. Sintering at 1450 °C (10 h dwelling time) leads to dense ceramic bodies with a relative bulk density of 91 %. Using the same sintering regime compacts made from a fine-grained $BaCeO_3$ powder (S_{BET} = 5.8 m^2/g) reach up to

1450 °C a relative density of 83 % as reported in [25]. It is to be noted that dense ceramic bodies from the nano-sized powder **1** are already obtained at sintering temperatures below 1480 °C, i.e. the peritectic temperature of $BaCeO_3$ [32].

The high sintering activity of powder **1** results from its nano-scaled morphology because of the large amount of grain boundaries, which promote sliding processes (rearrangement). Sliding processes are caused by amorphous or defect-rich grain boundaries [63,62]. *Dror* et al. [64] observed that a high amount of grain boundaries promotes sliding processes and they described the grain boundaries as amorphous areas surrounding crystalline cores.

Conclusion

We prepared nano-sized $BaCeO_3$ powders using a Ce^{4+}-salt and starch as a polymerization agent. The resulting (BaCe)-gel can be decomposed by a heating-rate controlled process at 920 °C to a phase-pure $BaCeO_3$ powder (**1**) with a specific surface area of 15.4 m^2/g and a crystallite size of about 41 nm. TEM images mainly show particles in the range of 30–65 nm. The nano-sized $BaCeO_3$ powder shows an improved sintering behaviour. Dilatometric measurements of compacts reveal that the beginning of the shrinkage is shifted below 1000 °C. Dense ceramic bodies (relative density ≥ 90 %) can be obtained after isothermal sintering at 1450°C (10 h) without any sintering additive.

Acknowledgements

The authors thanks Dr. Th. Müller for dilatometric and TG/DTA measurements.

Captions

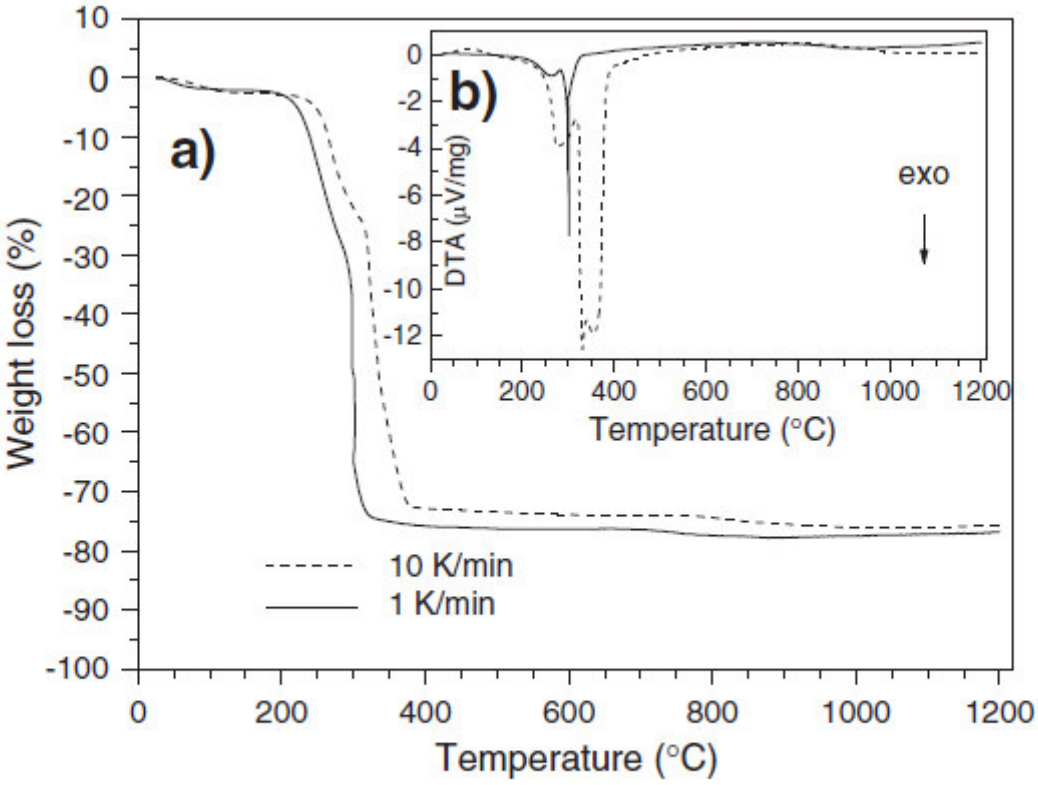

Fig. 1. Simultaneous TG (a) and DTA (b) curves of a preheated (BaCe)-gel in air up to 1200 °C with heating rates of 10 K/min and 1 K/min, respectively.

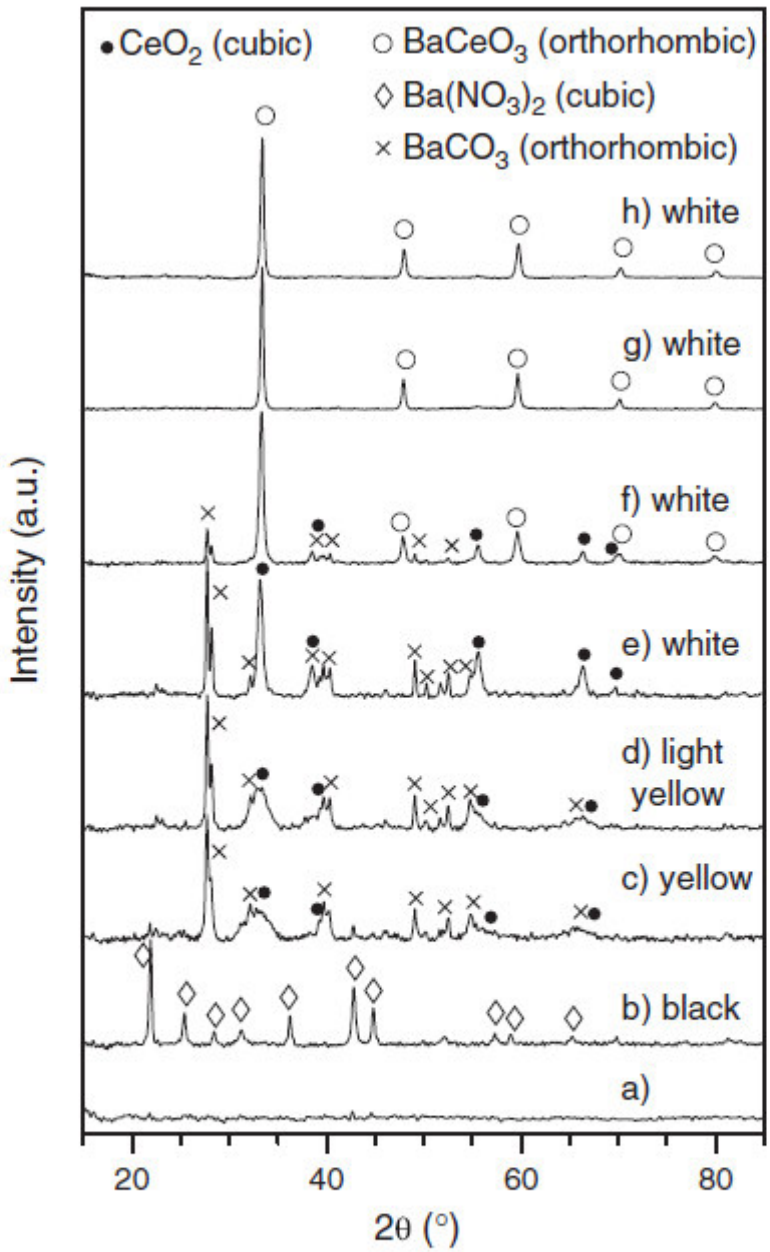

Fig. 2. Room temperature XRD patterns of the (BaCe)–gel (a) and calcination products (b–g) at various temperatures (soaking time 1 h, rate 10 K/min): b) 300 °C, c) 400 °C, d) 600 °C, e) 800 °C. f) 900 °C, g) 1000 °C, h) powder **1** from a heating rate controlled calcination process at 920 °C for 2 h.

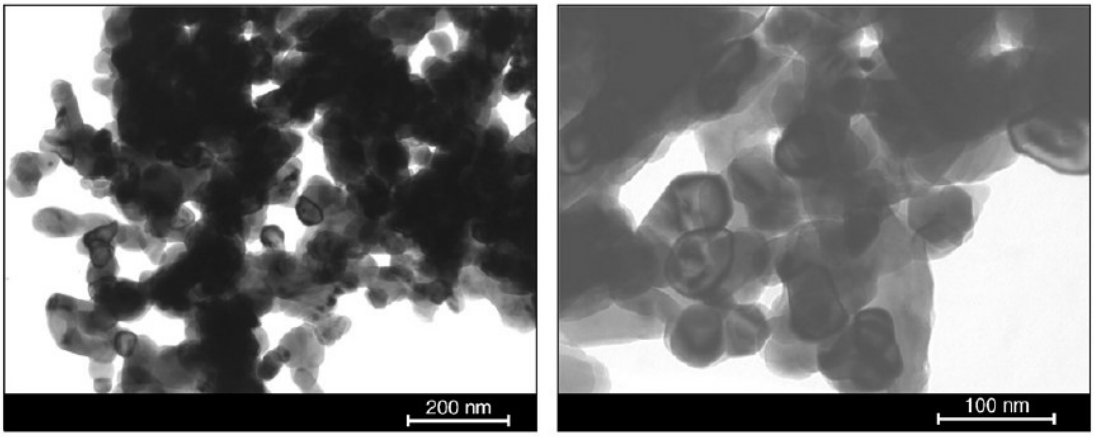

Fig. 3. TEM images of powder **1**.

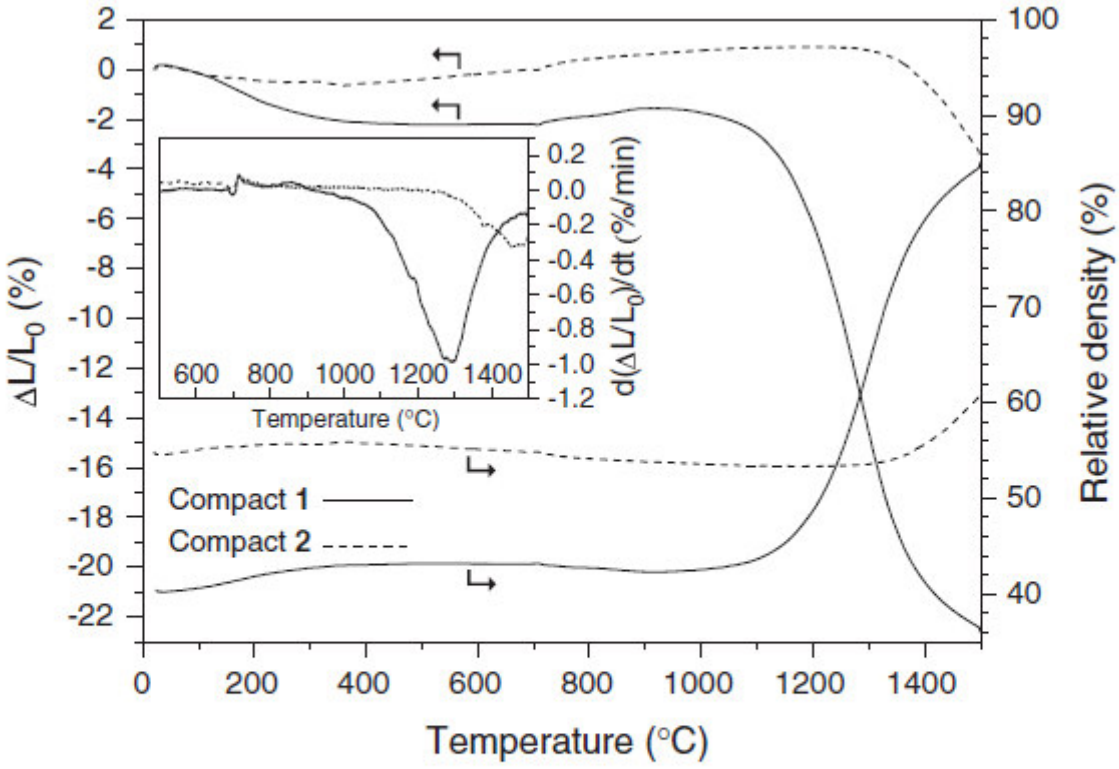

Fig. 4. Non-isothermal dilatometric measurements of green bodies of **1** and **2** in flowing air (heating rate 10 K/min). The relative densities were calculated assuming an isotropic shrinkage behavior. The inset shows the relative shrinkage rates ($d(\Delta L/L_0)/dt$). The green densities are 2.6 g/cm^3 (**1**) and 3.5 g/cm^3 (**2**), respectively.

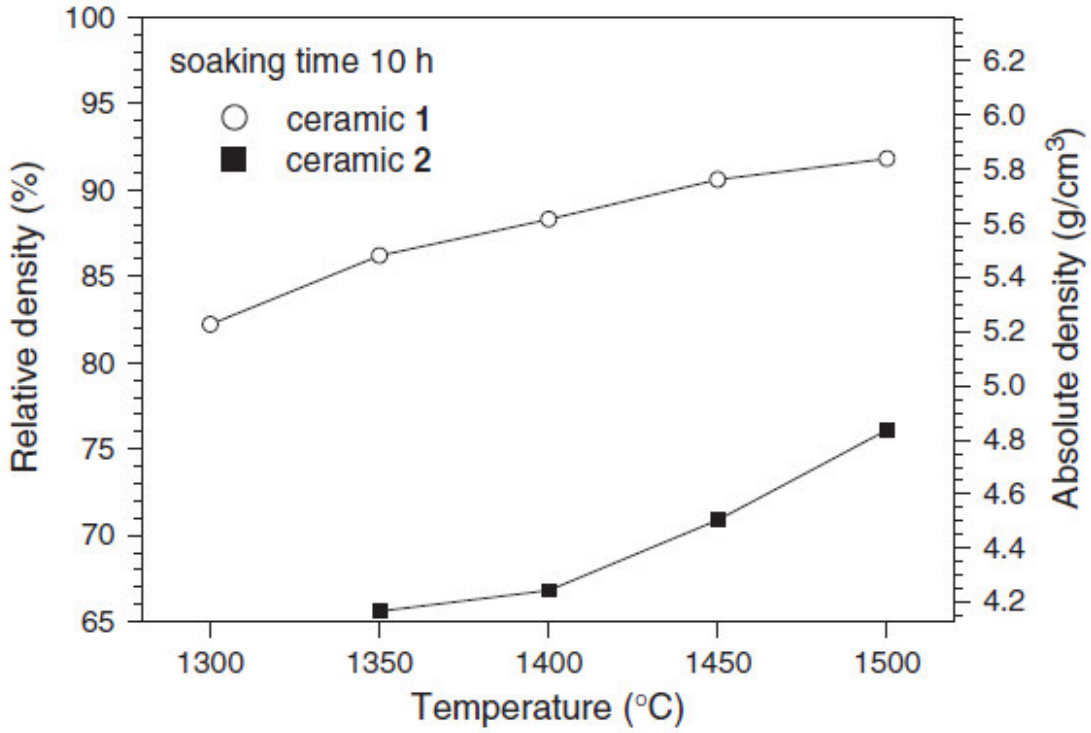

Fig. 5. Final bulk densities versus sintering temperature of ceramic bodies of **1** and **2** (soaking time: 10 h, heating-/cooling rate: 10 K/min).

References

[1] Z. Tao, Z. Zhu, H. Wang, W. Liu, J. Power Sources 195 (2010) 3481–3484.

[2] K. Künstler, H.-J.Lang, A. Maiwald, G. Tomandl, Solid State Ionics 107 (1998) 221–229.

[3] T. Scherban, W.-K. Lee, A.S. Nowick Solid State Ionics 28–30 (1988) 585–588.

[4] K. Katahira, Y. Kohchi, T. Shimura, H. Iwahara, Solid State Ionics 138 (2000) 91–98.

[5] K.H. Ryu, S.M. Haile, Solid State Ionics 125 (1999) 355–367.

[6] H. Iwahara, H. Uchida, K. Morimoto, J. Electrochem. Soc. 137 (1990) 462–465.

[7] Q. Ma, R. Peng, Y. Lin, J. Gao, G. Meng, J. Power Sources 161 (2006) 95–98.

[8] C.W. Tanner, A.V. Virkar, J. Electrochem. Soc. 143 (1996) 1386–1389.

[9] M.J. Scholten, J. Schoonman, J.C. van Miltenburg, H.A.J. Oonk, Solid State Ionics 61 (1993) 83–91.

[10] K. Xie, R. Yan, X. Chen, D. Dong, S. Wang, X. Liu, G. Menga, J. Alloy Compd. 472 (2009) 551–555.

[11] F. Zhao, Q. Liu, S. Wang, K. Brinkman, F. Chen, Int. J. Hydrogen Energ. 35 (2010) 4258–4263.

[12] T. Hibino, H. Iwahara, Sens. Actuators B13–14 (1993) 483–485.

[13] A. Chen, Y. Zhi, J. Zhi, P.M. Vilarinho, J.L. Baptista, J. Eur. Ceram. Soc. 17 (1997) 12–17.

[14] K. Komatsu (1997) Barium titanium cerium oxide dielectric ceramic composition with high dielectric constant and small dielectric constant shift by temperature changes. JP Patent No. 09157011 A.

[15] P. Baxter, N.J. Hellicar, B. Lewis, J. Am. Ceram. Soc. 42 (1959) 465–470.

[16] D. Kolar, J.P. Guha, M. Buh, Proc. Brit. Ceram. Soc. 23 (1972) 152–158.

[17] D.-Y. Lu, X.-Y. Sun, M. Toda, J. Phys. Chem. Solids 68 (2007) 650–664.

[18] A. Benlhachemi, K. Ouzaouit, H. Benyaich, S. Villain, J.R. Gavarri, Physical & Chemical News 41 (2008) 50–54.

[19] I. Popescu, I.-C. Marcu, I. Sandulescu, D. Macovei, Prog. Catal. 15 (2006) 79–85.

[20] X.-L. Yang, W.-Q. Zhang, C.-G. Xia, X.-M. Xiong, X.-Y. Mu, B. Hu, Catal. Commun. 11 (2010) 867–870.

[21] K. Ikeue, S. Kobayashi, M. Machida, J. Ceram. Soc. Jpn. 117 (2009) 1153−1157.

[22] Y. Yuan, J. Zheng, X. Zhang, Z. Li, T. Yu, J. Ye, Z. Zou, Solid State Ionics 178 (2008) 1711–1713.

[23] K.S. Knight, Solid State Ionics 74 (1994) 109−117.

[24] F. Genet, S. Loridant, C. Ritter, G. Lucazeau, J. Phys. Chem. Solids 60 (1999) 2009–2021.

[25] R. Köferstein, L. Jäger, S. G. Ebbinghaus, J. Mater. Sci. 45 (2010) 6521–6527.

[26] R.W. Rice, Porosity of Ceramics, ed. Marcel Dekker, New York, 1998, pp. 325 et seqq.

[27] Z. He, L. Ma, R. Zhang, Ceram. Int. 30 (2004) 1353–1356.

[28] D.M. Iddles, A.J. Bell, A.J. Moulson, J. Mater. Sci. 27 (1992) 6303−6310.

[29] N. Osman, I.A. Talib, H.A. Hamid, Ionics 15 (2009) 203–208.

[30] E. Gorbova, V. Maragou, D. Medvedev, A. Demin, P. Tsiakaras, J. Power Sources 181 (2008) 292–296.

[31] F.L. Chen, T. Sorensen, G.Y. Meng, D.K. Peng, J. Eur. Ceram. Soc. 18 (1998) 1389–1395.

[32] J.P. Guha, D. Kolar, J. Mater. Sci. 6 (1971) 1174−1177.

[33] R. Köferstein, L. Jäger, M. Zenkner, T. Müller, H.-P. Abicht, Mater. Chem. Phys. 112 (2008) 531−535.

[34] M. Zenkner, L. Jäger, R. Köferstein, H.-P. Abicht, Solid State Sci. 10 (2008) 1556−1562.

[35] A.V. Orlov, O.A. Shlyakhtin, A.L. Vinokurov, A.V. Knotko, Y.D. Tretyakov, Inorg. Mater. 41 (2005) 1194−1200.

[36] C.-J. Kim, N. Qadir, A. Mahmood, Y.-H. Han, T.-H. Sung, Physica C 463–465 (2007) 344–347.

[37] H. Muthurajan, N. Koteswara Rao, U.N. Gupta, S. Pradhan, R.K. Jha, H.H. Kumar, S.A. Mirji, V. Ravi, Mater. Res. Bull. 43 (2008) 1842–1849.

[38] M. Amsif, D. Marrero-López, A. Magrasó, J. Pena-Martínez, J.C. Ruiz-Morales, P. Núnez, J. Eur. Ceram. Soc. 29 (2009) 131–138.

[39] C. Xu, J. Zhu, X. Yang, L. Lu, X. Wang, J. Rare Earths 26 (2008) 51–54.

[40] J. Cai, K. Laubernds, F.S. Galasso, S.L. Suib, J. Liu, X.-F. Shen, E. Begge, H.R. Kunz, J.M. Fenton, J. Am. Ceram. Soc. 88 (2005) 2729–2735.

[41] A.P. Almeida de Oliveira, J. Hafsaoui, J.F. Hochepied, M.-H. Berger, A. Thorel, J. Eur. Ceram. Soc. 27 (2007) 3597–3600.

[42] H.-L. Lin, R.K. Chiang, C.-L. Kuo, C.-W. Chang, J. Non-Cryst. Solids 353 (2007) 1188–1194.

[43] D.W. Lee, J.H. Won, K.B. Shim, Mater. Lett. 57 (2003) 3346–3351.

[44] N. Osman, I.A. Talib, H. A. Hamid, Ionics 16 (2010)561–569.

[45] X.T. Su, Q.-Z. Yan, X.-H. Ma, W.-F. Zhang, C.-C. Ge, Solid State Ionics 177 (2006) 1041–1045.

[46] S. Bhowmick, J. Basu, Y. Xue, C. B. Carter, J. Am. Ceram. Soc. 93 (2010) 4041–4046.

[47] Q. Feng, X.H. Ma, Q.Z. Yan, C.C. Ge, Mater. Sci. Eng. B 162 (2009) 53–58.

[48] Z. Khani, M. Taillades-Jacquin, G. Taillades, M. Marrony, D.J. Jones, J. Roziere, J. Solid State Chem. 182 (2009) 790–798.

[49] M. Cernea, O. Monnereau, P. Llewellyn, L. Tortet, C. Galassi, J. Eur. Ceram. Soc. 26 (2006) 3241–3246.

[50] W. Kraus, G. Nolze, Powder Diffr. 13 (1998) 256–259.

[51] Th.H. De Keilser, E.J. Mittermeijer, H.C.E Rozendaal, J. Appl. Cryst. 16 (1983) 309−316.

[52] Program WinXPOW v1.06, Stoe & Cie GmbH, Darmstadt (1999).

[53] A.R. Stokes, A.J.C. Wilson, Proc. Phys. Soc. 56 (1944) 174−181.

[54] V.D. Allred, S.R. Buxton, J.P. McBride, J. Phys. Chem. 61 (1957) 117−120.

[55] PDF 2 (International Centre for Diffraction Data, Pennsylvania) 2001, $BaCeO_3$ [82-2425], $BaCO_3$ [5-378], CeO_2 [75-76], $Ba(NO_3)_2$ [76-1376].

[56] M.T. Buscaglia, M. Bassoli, V. Buscaglia, R. Alessio, J. Am. Ceram. Soc. 88 (2005) 2374–2379.

[57] V. D. Allred, S. R. Buxton, J. P. McBride, J. Chem. Phys. 61 (1957) 117–120.

[58] R. C. Garvie, J. Phys. Chem. 69 (1965) 1238–1243.

[59] K.S. Knight, N. Bonanos, Mater. Res. Bull. 30 (1995) 347–356.

[60] R. Köferstein, L. Jäger, M. Zenkner, S.G. Ebbinghaus, J. Eur. Ceram. Soc. 29 (2009) 2317–2324.

[61] R. Köferstein, L. Jäger, M. Zenkner, T. Müller, S.G. Ebbinghaus, J. Eur. Ceram. Soc. 30 (2010) 1419–1425.

[62] W. Schatt, Sintervorgänge. VDI-Verlag, Düsseldorf, 1992, pp. 78–100.

[63] W. Schatt, Z. Metallkde. 80 (1989) 809–816.

[64] Y. Dror, R. D. Levi, S. Baltianski, Y. Tsur, *J. Electrochem. Soc.*, 153 (2006) F137–F143.